

# Silicon nanoparticles generated by femtosecond laser ablation in a liquid environment

N. G. Semaltianos · S. Logothetidis · W. Perrie ·  
S. Romani · R. J. Potter · S. P. Edwardson ·  
P. French · M. Sharp · G. Dearden · K. G. Watkins

Received: 28 January 2009 / Accepted: 25 March 2009 / Published online: 10 April 2009  
© Springer Science+Business Media B.V. 2009

**Abstract** Silicon nanoparticles were generated by femtosecond laser [387 nm, 180 fs, 1 kHz, pulse energy = 3.5  $\mu\text{J}$  (fluence = 0.8  $\text{J}/\text{cm}^2$ )] ablation of silicon in deionized water. Nanoparticles with diameters from  $\sim 5$  up to  $\sim 200$  nm were observed to be formed in the colloidal solution. Their size distribution follows log-normal function with statistical median diameter of  $\approx 20$  nm. Longer ablation time leads to a narrowing of the nanoparticle size distribution due to the interaction of the ablating laser beam with the produced nanoparticles. Raman spectroscopy measurements confirm that the nanoparticles exhibit phonon quantum confinement effects and indicate that under the present conditions of ablation they are partially amorphous.

**Keywords** Silicon nanoparticles · Synthesis · Femtosecond laser ablation · Raman spectroscopy

---

N. G. Semaltianos (✉) · S. Logothetidis  
Department of Physics, Aristotle University of  
Thessaloniki, 54124 Thessaloniki, Greece  
e-mail: semal@physics.auth.gr

W. Perrie · S. Romani · R. J. Potter ·  
S. P. Edwardson · G. Dearden · K. G. Watkins  
Department of Engineering, University of Liverpool,  
Brownlow Hill, Liverpool L69 3GH, UK

P. French · M. Sharp  
General Engineering Research Institute,  
Liverpool John Moores University, Byrom Street,  
Liverpool L3 3AF, UK

## Introduction

Silicon nanoparticles are important nanomaterials both for applications in optoelectronics (Walters et al. 2005; Pavesi et al. 2000) but also as model systems for the study of fundamental quantum confinement effects (Mishra and Jain 2002; Richter et al. 1981; Campbell and Fauchet 1986; Meier et al. 2006, 2007). In particular Si/SiO<sub>2</sub> particles with diameters of 100 or 20 nm were found to increase the conductivity of the conjugated polymer poly(*p*-phenylene vinylene) (PPV) and produce a large blue shift in its absorption and luminescence spectra (Yang et al. 2005, 2007) while ultrasmall particles with diameters in the range 1–3 nm are used as red–green–blue (RGB) emitters in optoelectronic devices (Wang et al. 2008; Andsager et al. 1993). Thus, a number of methods have been developed for their production. Among them are silicon ion implantation into SiO<sub>2</sub> followed by annealing (Min et al. 1996; Linros et al. 1999), sputter deposition (Soni et al. 1999), rf plasma dissociation of argon–silane (SiH<sub>4</sub>) gas mixture (Mangolini et al. 2005; Takagi et al. 1990), electrochemical etching of crystalline silicon in a mixture of HF, H<sub>2</sub>O<sub>2</sub> and methanol (Wang et al. 2008; Andsager et al. 1993) and CO<sub>2</sub> laser pyrolysis of silane (Ledoux et al. 2000). Silicon nanoparticles have also been produced by laser ablation usually using long pulse (5–15 ns), low frequency (1–10 Hz) laser sources in the UV or green (193, 266 or 532 nm) (Hirasawa et al. 2004), in either controlled gas atmospheres

(Hirasawa et al. 2004; Makino et al. 2005; Patrone et al. 2000; Muramoto et al. 1999) or liquid environments (Umezumi et al. 2007). Recently, silicon nanoparticles have also been produced using a short pulse (picosecond) laser source (Wu et al. 2005).

This article involves the generation of silicon nanoparticles using an ultrashort pulse (femtosecond) laser source in a liquid environment. The produced nanoparticles colloidal solution was characterized by UV-spectrophotometry and the nanoparticles by transmission electron microscopy (TEM), atomic force microscopy (AFM) and Raman spectroscopy.

## Experimental details

In this work, a Ti:Sapphire femtosecond laser (Clark-MXR 2010) [wavelength ( $\lambda$ ) = 387.5 nm produced by frequency doubling of the 775 nm main laser beam using a BBO crystal, pulse width = 180 fs, frequency = 1 kHz] based on the chirped pulse amplification (CPA) technique (Strickland and Mourou 1985) was used for ablation of the target material. A schematic diagram of the experimental setup is shown in Fig. 1. The target material in the form of a square with dimensions of  $\sim 9.5 \times 9.5$  mm, thickness  $\sim 250$   $\mu\text{m}$  was positioned inside a cuvette (inner dimensions  $10 \times 10 \times 35$  mm) (Suprasil 300 quartz) and held firmly in place with a flexible thin teflon ring which was placed at the bottom of the cuvette, acting as a “spring” and pushing the sample onto its vertical wall. The cuvette was filled with liquid and sealed. It

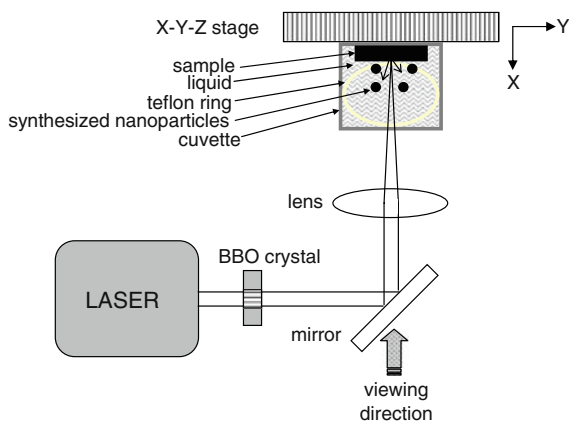


**Fig. 1** Schematic diagram (*top view*) of the experimental setup used for the generation of silicon nanoparticles by laser ablation of the target material in a liquid environment

was then placed onto an Aerotech moving stage which could be moved in the  $x$ ,  $y$  and  $z$  directions with accuracy of  $\pm 0.5$   $\mu\text{m}$ . The laser beam was focused onto the target material surface using a lens (focal length 5 cm). Laser ablation was carried out by scanning the sample (and thus the beam on its surface) with speed of 1 mm/s in a rectangular pattern with dimensions of  $9 \times 2.4$  mm and pitch of 0.005 mm (meander fashion scanning). No bubbles were observed to adhere onto the sample surface during ablation which would have otherwise shielded or scattered the laser radiation. The laser fluence was kept low at  $0.8$   $\text{J}/\text{cm}^2$  (laser pulse energy 3.5  $\mu\text{J}$ ). Deionized water (DIW) was used as the liquid. The sample was cut-out from an undoped (001) silicon wafer with resistivity  $>8,000$  Ohms cm. Ablation was carried out for  $\sim 70$  min and formation of nanoparticles in the solution could be confirmed by the slight change of the colour of the solvent during ablation. The total mass of the material ablated and transferred into the solvent as nanoparticles was estimated to be  $\sim 15$   $\mu\text{g}$ . All measurements were performed 1 day after preparation of the colloidal solution. TEM imaging of the nanoparticles was performed by drying out solution droplets onto carbon coated copper grids and using a high resolution JEOL JEM-3010 instrument. AFM imaging of the nanoparticles was performed by drying out droplets of the colloidal solution onto a clean hydrophilic silicon substrates, using a Veeco CP-II instrument in non-contact mode with Si cantilevers with a given radius of curvature  $<10$  nm (Tap300). Raman spectra were measured from the nanoparticles colloidal solution using a Jobin Yvon HR800 system (pumping beam at  $\lambda = 514.48$  nm) with a CCD detector. The colloidal solution was also characterized by UV-vis spectrophotometry.

## Results and discussion

The mechanism of formation of silicon nanoparticles by laser ablation of the target material in vacuum or controlled gas atmospheres using femtosecond laser pulses have been well studied in the literature both experimentally and theoretically (Perez and Lewis 2002; Cavalleri et al. 1999; Zhigilei 2003; Glover et al. 2003, 2004; Amoroso et al. 2005). According to a model which has been recently developed, it is

believed that the mechanism of formation of nanoparticles in the case of femtosecond laser ablation of a solid target is different than in the case of nanosecond laser ablation. This model predicts that the rapid transfer of energy from the carriers to the lattice due to the ultrashort pulse (isochoric lattice heating) has as a result that the material undergoes ultrafast non-thermal heating becoming a superheated fluid (Perez and Lewis 2002; Cavalleri et al. 1999). The building up of extreme thermoelastic pressure leads to material ejection directly in the form of nanoparticles (fragmentation model) (Zhigilei 2003; Glover et al. 2003, 2004). However, there are observations of nanoparticles with elemental compositions which deviated from the stoichiometry of the target material (formed together with the ones which they retained it) in thin films grown by femtosecond pulsed laser deposition of multi-element targets (alloys) (Perrière et al. 2007; Million et al. 2003). Besides, nanoparticles are observed with fundamentally different emission properties, formed during femtosecond laser ablation of single element targets, as compared to the droplets directly emitted from the target during nanosecond laser ablation (Albert et al. 2003). These lead to the conclusion that the mechanism of nanoparticle formation even in the case of femtosecond laser ablation might be similar to the case of nanosecond laser ablation. In the latter case, the nanoparticles are thought to be formed out by condensation in the vapour phase due to the adiabatic cooling of the expanding plasma plume. However, lately by combined molecular dynamics and direct simulation Monte Carlo (MD-DSMC) calculations (Itina et al. 2007) as well as from experiments on metallic targets (Nöel et al. 2007), it was concluded that both mechanisms play an important role in the formation of nanoclusters/nanoparticles during femtosecond laser ablation: the small particles (<7 nm) are directly ejected from the target while the larger particles are formed by collision-affected condensation and evaporation in the ablated plume flow. In our experiments, during laser ablation of the target materials a bright white colour “spot” could clearly be seen to be formed over the point of incidence of the laser beam onto the material surface. This spot corresponds to plasma plume of ablated species from the material because of the laser beam–material interaction. The

femtosecond pulse energy of 3.5  $\mu\text{J}$  which we use causes ablation of the material via sublimation. On the other hand, picosecond and especially nanosecond pulses will cause ablation of the material via vaporization and melting resulting in the formation of micron size particles (“liquid droplets”) which contribute to an overall broadening of the particle size distribution. By taking into account a  $9 \times 2.4$  mm ablated area, scanning speed of 1 mm/s (pitch 0.005 mm) and a measured ablation depth of  $\sim 100$  nm the surface enthalpy per pulse of the material during ablation is estimated equal to  $\sim 1 \times 10^9$  J/kg which is by two orders of magnitude larger than the sublimation (and therefore vaporization) enthalpy of  $1.6 \times 10^7$  J/kg for silicon (Glushko et al. 1990). Since the target material is immersed in the liquid, the liquid which is in contact with the material at the point of incidence of the laser beam onto the material surface is heated at the same very high temperature as the material surface. This results in the creation of vapours of the liquid. The loss of energy of the expanding plasma plume for the vaporization of the surrounding liquid and the additional pressure to the plume from the vapour of the liquid have as a result a decrease of the maximum expansion volume of the plume in a liquid environment as compared to air or vacuum expansion. This results in a higher nucleation rate resulting in the formation of a distribution of nanoparticles with a lower average diameter than in the case of air or vacuum expansion.

Figure 2 shows the optical absorption edge from the colloidal solution in the low energies region around the band gap of bulk Si.  $(\alpha\omega)^{1/2}$  is plotted versus  $\hbar\omega$  (where  $\alpha$  is the measured absorption coefficient). Silicon nanoparticles generated so far by laser ablation (using long pulse lasers) or with other methods were confirmed to be indirect band gap semiconductors (Meier et al. 2007; Makino et al. 2005; Umezu et al. 2007). Thus, assuming that the nanoparticles generated here by femtosecond laser ablation are also indirect band gap semiconductors, from the plot of Fig. 2 we can calculate their band gap energy ( $E_g$ ) according to the relation:

$$\alpha(\hbar\omega) \propto \omega^{-1}(\hbar\omega - E_g)^2 \quad (1)$$

which is valid for indirect band gap semiconductors. Linear fitting yields  $E_g = 1.2$  eV which corresponds

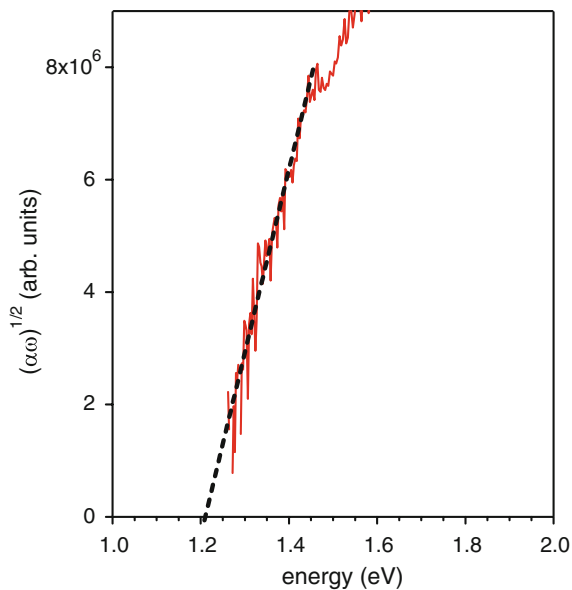


**Fig. 2** Optical absorption edge from the nanoparticles colloidal solution in the low energies region

to a blue shift of 0.08 eV from the band gap of  $E_0 = 1.12$  eV of bulk Si due to the effect of quantum confinement. From photoluminescence results and calculations using the linear combination of atomic orbitals (LCAO) technique, it was found that the band gap of Si nanoparticles as a function of the diameter  $d$  is described by the relation:

$$E_g = E_0 + \left( \frac{3.73}{d^{1.39}} \right) \quad (2)$$

(Delerue et al. 1993; Meier et al. 2007; Ledoux et al. 2000). Note that the effective mass theory would have resulted in a  $d^{-2}$  dependence, instead. From this relation, the above blue shift implies nanoparticles with diameter of  $d \approx 15.8$  nm.

Detailed information about the size distribution of the nanoparticles in the produced colloidal solution was obtained by TEM and AFM images (typical images are shown in Fig. 3). The histogram of particle size distribution (shown in Fig. 4a by counting approximately 350 particles in images of particles ensembles obtained on different areas on the grid) is described quite well by a log-normal function with median diameter of  $d_0 \approx 20$  nm and geometrical standard deviation  $\sigma \approx 0.81$ . Under the present conditions of laser ablation, a rather wide nanoparticle size distribution is obtained including particles

with diameters from  $\sim 5$  up to  $\sim 200$  nm. The larger median diameter (of  $d \approx 20$  nm) which is deduced from the TEM images as compared to the diameter ( $d \approx 15.8$  nm) estimated from the spectrophotometry data of Fig. 2, might be due to the fact that very small particles are not easily distinguished in the TEM images because they do not appear with high enough contrast and thus they are not included in the statistical distribution. This results in an overestimation of the average nanoparticle diameter from histograms calculated from TEM images.

During production of nanoparticles by laser ablation of target materials in liquid environments the newly produced nanoparticles lie unavoidably in the path of the ablating laser beam and thus there might interact with the laser beam. At the present case of femtosecond (ultrashort) pulse laser ablation this interaction is via “interpulse” absorption, i.e. absorption from particles of laser pulses subsequent to the ones by which the particles were created (Tsuji et al. 2002). Note that in the case of picosecond or longer pulse ablation the interaction of the produced particles with the laser beam is via “intrapulse” absorption, i.e. absorption from particles of part of the same laser pulse from which the particles were created. These interactions in turn offer the possibility of tuning the width of the nanoparticle size distribution, which are produced by laser ablation. This effect is demonstrated here by the histogram of Fig. 4b which corresponds to a nanoparticle size distribution in a colloidal solution which was produced by ablating the target material for a time duration of  $\sim 45$  min (smaller than the ablation time duration which produced the distribution corresponding to Fig. 4a). Because of the  $d^3$  dependence of the absorption cross section on particle size, in a given colloidal solution the larger nanoparticles absorb the laser beam stronger than the smaller ones and this results in a larger ablation rate of the larger particles as compared to the ablation rate of the smaller ones. This in turn results in a shift of the nanoparticle size distribution towards smaller diameters (Procházka et al. 1997).

The vibrational properties of the silicon nanoparticles produced by femtosecond laser ablation were investigated by measuring their Raman spectra. The transverse optical (TO) phonon line which from bulk silicon appears at  $522 \text{ cm}^{-1}$  (FWHM  $\approx 4 \text{ cm}^{-1}$ )

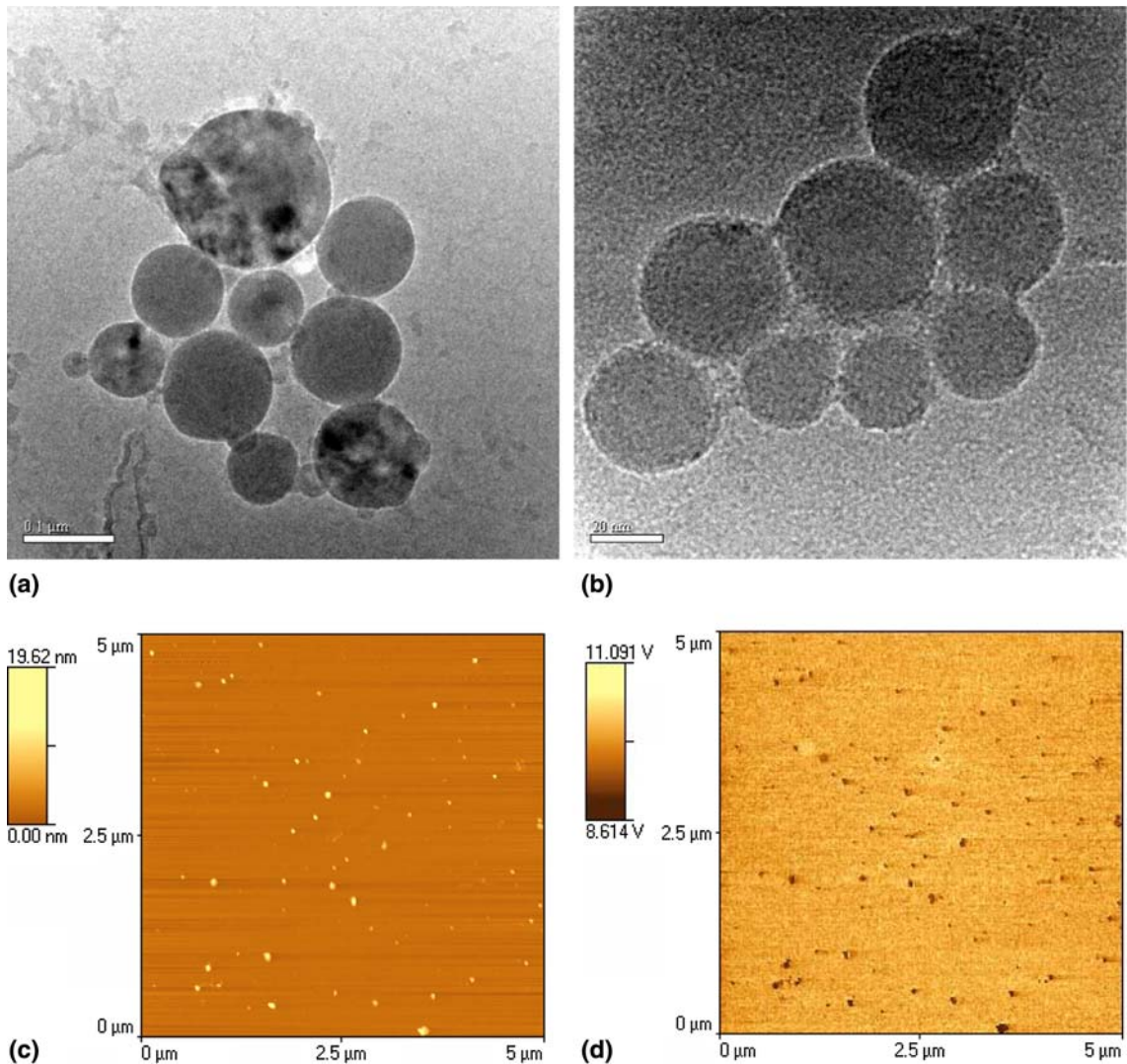
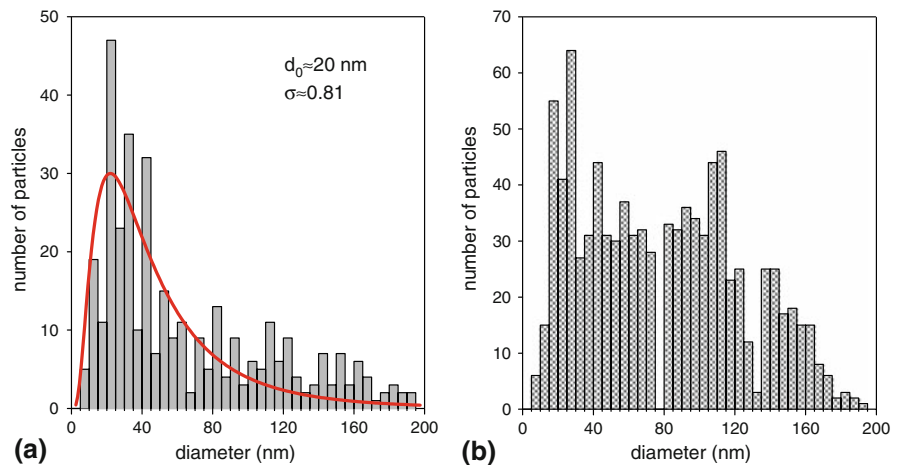


**Fig. 3** **a, b** Typical TEM and **c** AFM images of the nanoparticles. The image in **(d)** is the phase image corresponding to the topography image in **(c)**

(green line in Fig. 5), from the nanoparticles appears at  $520\text{ cm}^{-1}$  and with  $\text{FWHM} \approx 7.5\text{ cm}^{-1}$  (circle points in Fig. 5). This shift to lower wave numbers and broadening of the TO phonon line from the nanoparticles is due to the phonon quantum confinement effect (Richter et al. 1981; Campbell and Fauchet 1986). The origin of this effect lies to the fact that the break up of a long range order for the system of the nanoparticles results in a “softening” of the strict  $\Delta q = 0$  selection rule which applies to the case of a bulk crystal. The increase in the phonon localization because of their confinement in the nanoparticles results in a decrease of their

momentum determination (according to the uncertainty principle). Thus in that case, transitions from a broader interval around the centre of the Brillouin zone are also allowed. The Raman band is in fact a reflection of the optical phonon dispersion in  $q$ -space. In addition, a broad band appears at  $\sim 490\text{ cm}^{-1}$  and this band is a characteristic of an amorphous phase of silicon (Bermejo and Cardona 1979). This indicates that the produced silicon nanoparticles are partially amorphous (Hirasawa et al. 2004). The TO phonon Raman line intensity from silicon nanocrystallites is described mathematically by the relation:

**Fig. 4** Histograms of the nanoparticles size distributions



$$I(\omega) = \int_0^1 \frac{\exp(-q^2 d^2 / 4a^2)}{[(\omega - \omega(q))]^2 + (\Gamma/2)^2} d^3 q \quad (3)$$

(Richter et al. 1981; Campbell and Fauchet 1986) where  $d$  is the nanoparticle diameter,  $a = 5.34 \text{ \AA}$  is the lattice constant of bulk silicon and  $\Gamma = 4 \text{ cm}^{-1}$  is the linewidth of the TO phonon in bulk silicon. The dispersion  $\omega(q)$  of the TO phonon is given by the relation:

$$\omega^2(q) = A + B \cos(\pi q/2) \quad (4)$$

where  $A = 1.714 \times 10^5 \text{ cm}^{-2}$  and  $B = 1.000 \times 10^5 \text{ cm}^{-2}$  (Kanemitsu et al. 1993). The red line in Fig. 5 corresponds to fitting the above relation to the

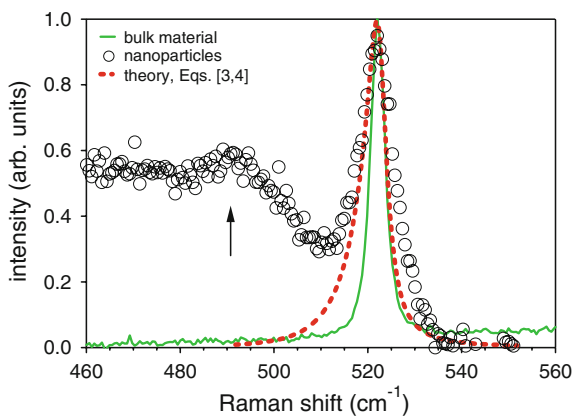


**Fig. 5** Raman spectra from bulk silicon as well as from the nanoparticles and theoretical curve calculated numerically using Eqs. 3 and 4

experimentally measured circle points, assuming nanoparticles with diameter  $d = 15 \text{ nm}$ .

## Conclusions

Silicon nanoparticles were produced by femtosecond laser ablation [387 nm, 180 fs, 1 kHz, pulse energy = 3.5  $\mu\text{J}$  (fluence = 0.8  $\text{J}/\text{cm}^2$ )] in DIW. The ultrashort pulses cause ablation of the material via sublimation and the interaction of the produced nanoparticles with the ablating laser beam is via “interpulse” absorption only. This interaction leads to a narrowing of the particle size distribution. The produced nanoparticles under the present conditions of ablation have sizes from  $\sim 5$  up to  $\sim 200 \text{ nm}$  with a statistical median diameter of  $\approx 20 \text{ nm}$ . The possibility of tuning the width of the nanoparticle size distribution by changing the ablation time duration is demonstrated. The produced nanoparticles exhibit phonon quantum confinement effects and consistency with the optical absorption measurements is found.

**Acknowledgements** N.G.S. acknowledges support by a Marie Curie European Reintegration Grant (ERG), contract number: PERG03-GA-2008-226029, 83573 under the project OMALANP.

## References

Albert O, Roger S, Glinec Y, Loulergue JC, Etchepare J, Boulmer-Leborgne C, Perrière J, Million E (2003)

- Time-resolved spectroscopy measurements of a titanium plasma induced by nanosecond and femtosecond lasers. *Appl Phys A* 76(3):319–323
- Amoruso S, Ausanio G, Barone AC, Bruzzese R, Gragnaniello L, Vitiello M, Wang X (2005) Ultrashort laser ablation of solid matter in vacuum: a comparison between the picosecond and femtosecond regimes. *J Phys B At Mol Opt Phys* 38:L329–L338
- Andsager D, Hilliard J, Hetrick JM, AbuHassan LH, Plisch M, Nayfeh MH (1993) Quenching of porous silicon photoluminescence by deposition of metal adsorbates. *J Appl Phys* 74:4783–4785
- Bermejo D, Cardona M (1979) Raman scattering in pure and hydrogenated amorphous germanium and silicon. *J Non Crystal Sol* 32:405–419
- Campbell IH, Fauchet PM (1986) The effects of microcrystal size and shape on the one phonon Raman spectra of crystalline semiconductors. *Solid State Commun* 58(10):739–741
- Cavalleri A, Sokolowski-Tinten K, Bialkowski J, Schreiner M, von der Linde D (1999) Femtosecond melting and ablation of semiconductors studied with time of flight mass spectroscopy. *J Appl Phys* 85(6):3301–3309
- Delerue C, Allan G, Lannoo M (1993) Theoretical aspects of the luminescence of porous silicon. *Phys Rev B* 48(15):11024–11036
- Glover TE, Ackerman GD, Belkacem A, Heimann PA, Hussain Z, Lee RW, Padmore HA, Ray C, Schoenlein RW, Steele WF, Young DA (2003) Metal-insulator transitions in an expanding metallic fluid: particle formation kinetics. *Phys Rev Lett* 90(23):236102–1–4
- Glover TE, Ackerman GD, Lee RW, Young DA (2004) Probing particle synthesis during femtosecond laser ablation: initial phase transition kinetics. *Appl Phys B* 78:995–1000
- Glushko VP, Gurvich LV, Veyts IV, Alock CB (1990) Thermodynamic properties of individual substances: elements and compounds. Taylor and Francis, London
- Hirasawa M, Orii T, Seto T (2004) Effect of insitu annealing on physical properties of Si nanoparticles synthesized by pulsed laser ablation. *Appl Phys A* 79:1421–1424
- Itina TE, Gouriet K, Zhigilei LV, Noël S, Hermann J, Sentis M (2007) Mechanisms of small clusters production by short and ultra-short laser ablation. *Appl Surf Sci* 253(19):7656–7661
- Kanemitsu Y, Uto H, Masumoto Y, Matsumoto T, Futagi T, Mimura H (1993) Microstructure and optical properties of free-standing porous silicon films: size dependence of absorption spectra in Si nanometer-sized crystallites. *Phys Rev B* 48(4):2827–2830
- Ledoux G, Guillois O, Porterat D, Reynaud C, Huisken F, Kohn B, Paillard V (2000) Photoluminescence properties of silicon nanocrystals as a function of their size. *Phys Rev B* 62(23):15942–15951
- Linros J, Lalic N, Galeckas A, Grivickas V (1999) Analysis of the stretched exponential photoluminescence decay from nanometer-sized silicon crystals in SiO<sub>2</sub>. *J Appl Phys* 86:6128–6134
- Makino T, Inada M, Umezu I, Sugimura A (2005) Structural and optical properties of surface-hydrogenated silicon nanocrystallites prepared by reactive pulsed laser ablation. *J Phys D Appl Phys* 38:3507–3511
- Mangolini L, Thimsen E, Kortshagen U (2005) High-yield plasma synthesis of luminescent silicon nanocrystals. *Nano Lett* 5:655–659
- Meier C, Lüttjohann S, Kravets VG, Nienhaus H, Lorke A, Wiggers H (2006) Raman properties of silicon nanoparticles. *Physica E* 32:155–158
- Meier C, Gondorf A, Lüttjohann S, Lorke A, Wiggers H (2007) Silicon nanoparticles: Absorption, emission, and the nature of the electronic bandgap. *J Appl Phys* 101:103112-1-7
- Million E, Perrière J, Défourneau RM, Défourneau D, Albert O, Etchepare J (2003) Femtosecond pulsed-laser deposition of BaTiO<sub>3</sub>. *Appl Phys A* 77(1):73–80
- Min KS, Shcheglov KV, Yang CM, Atwater HA, Brongersma ML, Polman A (1996) Defect-related versus excitonic visible light emission from ion beam synthesized Si nanocrystals in SiO<sub>2</sub>. *Appl Phys Lett* 69:2033–2035
- Mishra P, Jain KP (2002) Raman, photoluminescence and optical absorption studies on nanocrystalline silicon. *Mat Sci Eng B* 95(3):202–213
- Muramoto J, Inmaru T, Nakata Y, Okada T, Maeda M (1999) Influence of ambient gas on formation process of Si nanoparticles by laser ablation. *Appl Phys A* 69:S239–S241
- Noël S, Hermann J, Itina T (2007) Investigation of nanoparticle generation during femtosecond laser ablation of metals. *Appl Surf Sci* 253(15):6310–6315
- Patrone L, Nelson D, Sfarov VI, Sentis M, Marine W (2000) Photoluminescence of silicon nanoclusters with reduced size dispersion produced by laser ablation. *J Appl Phys* 87:3829–3837
- Pavesi L, Dal Negro L, Mazzoleni C, Franco G, Priolo F (2000) Optical gain in silicon nanocrystals. *Nature* 408:440–444
- Perez D, Lewis LJ (2002) Ablation of solids under femtosecond laser pulses. *Phys Rev Lett* 89(25):255504-1-4
- Perrière J, Boulmer-Leborgne C, Benzerga R, Tricot S (2007) Nanoparticle formation by femtosecond laser ablation. *J Phys D Appl Phys* 40:7069–7076
- Procházka M, Mojžeš P, Štěpánek J, Vlčková B, Turpin P-Y (1997) Probing applications of laser-ablated Ag colloids in SERS spectroscopy: improvement of ablation procedure and SERS spectral testing. *Anal Chem* 69:5103–5108
- Richter H, Wang ZP, Ley L (1981) The one phonon Raman spectrum in microcrystalline silicon. *Solid State Commun* 39:625–629
- Soni RK, Fonseca LF, Resta O, Buzaianu M, Weisz SZ (1999) Size-dependent optical properties of silicon nanocrystals. *J Lumin* 83–84:187–191
- Strickland D, Mourou G (1985) Compression of amplified chirped optical pulses. *Opt Commun* 56(3):219–221
- Takagi H, Ogawa H, Yamazaki Y, Ishizaki A, Nakagiri T (1990) Quantum size effects on photoluminescence in ultrafine Si particles. *Appl Phys Lett* 56:2379–2380
- Tsuji T, Iryo K, Watanabe N, Tsuji M (2002) Preparation of silver nanoparticles by laser ablation in solution: influence of laser wavelength on particle size. *Appl Surf Sci* 202:80–85
- Umezu I, Minami H, Senoo H, Sugimura A (2007) Synthesis of photoluminescent colloidal silicon nanoparticles by pulsed laser ablation in liquids. *J Phys Conf Ser* 59:392–395

- Walters RJ, Bourianoff GI, Atwater HA (2005) Field-effect electroluminescence in silicon nanocrystals. *Nat Mater* 4:143–146
- Wang G, Yau ST, Mantey K, Nayfeh MH (2008) Fluorescent Si nanoparticle-based electrode for sensing biomedical substances. *Opt Commun* 281:1765–1770
- Wu MH, Mu R, Ueda A, Henderson DO, Vlahovic B (2005) Production of silicon quantum dots for photovoltaic applications by picosecond pulsed laser ablation. *Mat Sci Eng B* 116:273–277
- Yang SH, Nguyen TP, Le Rendu P, Hsu CS (2005) Optical and electrical properties of PPV/SiO<sub>2</sub> and PPV/TiO<sub>2</sub> composite materials. *Compos Part A Appl Sci Manuf* 36(4):509–513
- Yang SH, Le Rendu P, Nguyen TP, Hsu CS (2007) Fabrication of MEH-PPV/SiO<sub>2</sub> and MEH-PPV/TiO<sub>2</sub> nanocomposites with enhanced luminescent stabilities. *Rev Adv Mater Sci* 15:144–149
- Zhigilei LV (2003) Dynamics of the plume formation and parameters of the ejected clusters in short-pulse laser ablation. *Appl Phys A* 76:339–350